



Honors Theses at the University of Iowa

Spring 2017

The Design of an Electro-Mechanical Bicycle for an Immersive Virtual Environment

Oliver Stroh
University of Iowa

Follow this and additional works at: https://ir.uiowa.edu/honors_theses



Part of the [Electro-Mechanical Systems Commons](#), [Industrial Engineering Commons](#), and the [Systems Engineering Commons](#)

This honors thesis is available at Iowa Research Online: https://ir.uiowa.edu/honors_theses/89

THE DESIGN OF AN ELECTRO-MECHANICAL BICYCLE FOR AN IMMERSIVE VIRTUAL
ENVIRONMENT

by

Oliver Stroh

A thesis submitted in partial fulfillment of the requirements
for graduation with Honors in the Industrial Engineering

Geb W. Thomas
Thesis Mentor

Spring 2017

All requirements for graduation with Honors in the
Industrial Engineering have been completed.

Geb W. Thomas
Industrial Engineering Honors Advisor

Abstract

Roughly 50,000 people are injured in bicycle collisions with motor vehicles each year, approximately 6,000 of these injuries involve children less than 14 years old. To better understand which factors put bicycling children at risk for motor vehicle collisions, researchers at the University of Iowa built a virtual environment that simulates the experience of riding through a town and crossing roads with motor vehicles traffic. The stationary bicycle, the focus of this report, replicates the pedal forces experienced by a rider. The stationary bike also provides the simulator with the bicycle's velocity and steering angle. This report describes the design of the system, which features a flywheel designed to represent the rider and bike inertia, the mechanical linkages between the rider and an electric motor, and a system to measure steering angles. The bicycle has been built and tested and is currently in use in the virtual environment.

Table of Contents

1. Introduction	1
2. Literature Review	2
3. Background.....	5
3.1. Physics of Bicycling.....	5
3.2. Past Iterations for Hank Simulator	7
4. Methods	7
4.1. Selecting the Bicycles	8
4.2. Simulating Kinetic Energy	10
4.3. Simulating Wind Resistance	12
4.4. Integration With Bikes	13
4.5. Spinning the Front Wheel	17
4.6. Measuring Steering Angle.....	21
4.7. Electrical Communication.....	22
5. Results	23
6. References	24

1. Introduction

Bicycles have been around since the early 1800's, but with the invention of motor vehicles nearly 70 years later the risk for bicycle injuries has increased. Approximately 6,000 children less than 14 years old are injured in bicycle-motor vehicle collisions every year. Fifty such collisions each year result in child fatalities (National Center Statistics, 2016). In 2010, there was an estimated lifetime medical cost of 10 billion dollars due to fatal and non-fatal bicycle-crash related injuries (Center for Disease Control and Prevention, 2016). Virtual reality provides a unique opportunity to safely investigate in children in traffic heavy settings. The Hank bicycle simulator has been instrumental in this type of investigation for over a decade and has provided unique insights into the perceptions and decision-making process of children and adults encountering traffic on a bicycle (Grechkin et al, 2013; Plumert, Kearney and Cremer, 2004; Plumert, Kearney and Cremer, 2007). Analyzing the simulation data allows researchers to understand what factors put children at risk for motor-vehicle collisions.

The Hank simulator includes an instrumented bicycle fixed in the center of a three projection screens and a projection floor (Babu, Grechkin, et al., 2009). The movement of the bicycle is synchronized with graphics so that the rider is presented with a three-dimensional view consistent with riding through a town or countryside. A typical simulation setting is showing a street on the simulator screens and instructing a bicyclist to cross the street when they deem appropriate. This puts high demand on the accuracy of the stationary bicycle used in the simulator as the initial acceleration period is critical to accurate simulation. As a result, this study seeks to design a bicycle for riding through a virtual environment. The bike should provide the

steering angle and velocity to the virtual environment simulator, accurately resist pedal movement, and spin the front wheel to simulate typical bike interaction.

2. Literature Review

Several researchers have implemented similar devices in several ways. Some are most interested in the influence of virtual reality on exercise (Huang et al. 2008; Mestre, Dagonneau and Mercier, 2011). Others are most interested on the mathematical details of the control system (Leblanc and Sicard, 2010). Still others are interested primarily as using a bike as method for pleasantly moving through a virtual environment (Sari et al., 2009). Our interest is primarily in the construction of a working bicycle with sufficient fidelity to reconstruct the force-displacement relationship in real time to serve as a platform for psychological experiments involving decision-making.

Table 1 shows five other bicycle simulators featuring controlled pedal resistance. The KAIST simulator (Kwon et al., 2001; Kwon et al., 2002) was designed to completely immerse a rider in a bicycle race with other riders on similar bicycles. It features a bicycle mounted on a six-degree-of-freedom Stewart platform, with motions emphasizing the vertical movement (heave), but also supporting side-to-side (roll) and front-to-rear (pitch) movements. Pedal resistance is provided through a magneto-rheological fluid brake (MRB). An AC servomotor produced acceleration due to gravity. The rider wears a head-mounted display (HMD) and graphics are synchronized with a second bicycle over a network.

The Hong Kong system (Tang et al., 2007) was designed to promote exercise through cycling. The dense population of the city provided an insufficient amount of space for people exercising outdoors. Their bicycle simulator allows multiple riders to exercise in a confined space. The bicycle rests on a platform with springs supporting the bottom that allowed the riders

to slightly tilt as they would pedal and turn. A damper is attached to the rear wheel to provide resistance due to wind and the different frictions of the road surfaces. An AC servomotor produces decelerating or accelerating torque based on the slope of the rider's environment.

The Morics system (Miyanoue et al., 2015) was designed for traffic safety education and safety analysis among many different traffic situations. Morics can slightly lean to either side due to the rear wheel stand, however it does not provide a natural lean that a rider feels on turns. There is a load generator that creates the pedaling resistance based on the rider. An actuator produces resistance based on the current environment the rider is in, however it doesn't provide any wind resistance as the rider pedals. This study is concerned with the safety maneuvers a rider displays on the road with traffic present.

The Shanghai system (He et al., 2005) was designed to provide a complete two-wheeled bicycle dynamic model. Using Lagrange's equation of motion and the Runge-Kutta method they were successfully able to produce a mathematical model of a bicycle. The model consisted of two sub-models, the stability sub-model and the vibration sub-model. The stability sub-model solves the equations for the rider's current movement of the bicycle. The vibration sub-model solves the equations for the vibrations using the riding surface. The sub-models were verified by collected data on an actual bicycle ride through different surfaces. They collected the data of the steering angle, simulated tilt angle, measured tilt angle, vibration acceleration on different surfaces, and the velocity.

Bike Simulators					
	Kwon et al.	Tang et al.	Miyanoue et al.	He et al.	Kikuchi et al.
	KAIST	Hong Kong	Morics	Shanghai	Japan
Screen	Mono Display or HMD	Stereoscopic Display	Mono Display or HMD	HMD	Stereoscopic Display or HMD
Horizontal Field of View	45° or less	45° or less	102°	45° or less	45° or less
Vertical Field of View	45° or less (no ground)	45° or less	64°	45° or less (no ground)	45° or less
Sound	✓ (3D)	✓	✓	✓ (3D)	✓
Air Resistance	✓	✓	✗	✓	✓
Leaning	✓ (6-dof/4-dof)	✓ (Springs)	✓ (Not full range)	✓ (6-dof)	✗
Simulated Inertia	✓	✓	✓	✓	✓
Steering Angle	Max	Max	Max	Max	Max
Movement System Type	MR-Brake & AC Servomotor	Damper & AC Servomotor	Load Generator & Actuator	3 Torque Estimators	MRB
Front Wheel Velocity	✗ (No front wheel)	✗	✗	✗ (No front wheel)	✗
Instantaneous Inertia	Electronic Delay	Electronic Delay	Electronic Delay	Electronic Delay	Electronic Delay

Table 1: Bicycle simulators throughout the world

Table 1 compares several main features of each of the reference systems. Screen refers to the how the data are displayed and whether the presentation is 2D or 3D, the number of surrounding screens or a whether the implementation used a head-mounted display. All implementations included sound, though just two provide 3D sound. Four simulators allow the bicycle to tilt side to side, though one provides this mechanism with springs only. All implementations simulate the inertia of the rider.

In each of the five reference systems, the bicycles provide programmable, dynamic pedal resistance while providing steering angle and velocity to the graphical simulator system. Because our research problem emphasizes how people, particularly children, choose when to cross a street with traffic, we are particularly interested in creating a valid behavior for children and adult riders starting from a stopped position. Consequently, the relationship between the force applied to the pedals and the distance traveled is particularly important, since a rider presumably predicts where they will be a future time, based on how the bicycle will respond to their applied effort. We have not yet determined how exactly a rider perceives their own application of force, such as whether they remember the force relationship of their usual bicycle compared to the one in the simulator, or to what degree they are sensitive to subtle performance differences from one

trial to the next. In the past, we have been satisfied with pedal feedback that seemed realistic enough to not draw the attention of the riders, but in this work, we seek to quantify the performance of the system so that it might be compared against other systems.

3. Background

This section will cover some of the physics of bicycling, as well as discuss the advantages and disadvantages of previous simulator iterations.

3.1. Physics of Bicycling

A bicycle moves when the rider transfers energy to the pedals, causing a propulsive force, F_P , to act between the rear wheel and the ground. Generally speaking, this propulsive force accelerates the bike and rider when it overcomes the air resistance, F_A , the slope resistance, F_s , the rolling resistance between the tires and the ground, F_R , and the bump resistance, F_B . This results in the following force equation (Wilson and Papadopoulos, 2004):

$$ma = F_{acc} = F_P - (F_A + F_s + F_R + F_B)$$

where m is the mass and a is the acceleration of the bicycle and rider. The target simulation is assuming the rider is on smooth pavement, with no slope or head wind. Therefore the potential effects of rolling, slope, bump, and headwind resistance can be ignored (Wilson and Papadopoulos, 2004). This fully removed the terms F_s , F_R , and F_B . With no headwind the term F_A is reduced to the force of drag created by moving through air. The faster the bicycle can

accelerate, the quicker the rider can move across the street, reducing the rider's exposure to traffic. Consequently, the electro-mechanical bike should exhibit realistic acceleration, so that decisions research participants make about timing and exerted effort are relevant to the decisions they would make when in the real world. Also, the bicycle's motion should be consistent, so that experience in earlier trials can accurately inform the rider's expectation of behavior in future trials.

The resistance of the gear train, F_M , and between the tires and the ground, F_R , are relatively small effects for a well-maintained bicycle on pavement. Because aerodynamic drag increases with the square of the relative velocity between the bike and the air, drag is also small at low speeds. Thus, when considering the problem of crossing an intersection in a town, the problem of simulating the resistance to pedaling is mostly related to overcoming the inertia of the rider and bicycle. This results in the above function simplifying to:

$$ma \approx F_p$$

Thus, the main factor determining the rider's forward progress during the first few moment of movement is inertia, more specifically the rider's mass, since other person-dependent variables such as their anthropometrics are covered within the sizes of the bikes and have no bearing on them attempting to cross the road. Simulating the inertia, then, is the most critical component of reproducing appropriate forces in the specific application of choosing when to cross a street from a complete stop.

3.2. Past Iterations for Hank Simulator

The first two iterations of the Hank Simulator bicycle relied on a large roller placed in contact with the back tire. The roller effectively reproduced the contact with the ground. The relatively large size and mass of the 6.5” diameter aluminum roller provided inertia in the system, but this inertia was not carefully accounted for in the rest of the programming. The primary control was a large motor connected to the roller. The motor controller was programmed in velocity control mode. When the rider began to pedal, both the bicycle motor speed and the power consumed by the motor to maintain the current velocity would be sent to a microprocessor. The microprocessor calculated the power required by a rider moving at the speed to overcome wind drag, calculated an acceleration based on the current power required, and updated the motor velocity command accordingly. The inertial terms were effectively ignored by this calculation; all the emphasis was on the steady-state motion. This situation persisted for several years because the large roller provided enough inertia that people generally didn’t notice that they were able to accelerate independently from their mass, once several other terms in the model had been adjusted in order to make the bike feel “realistic.”

It would be possible to simulate the inertia by adding a term to the motor controller that was sensitive to the change in velocity over time. Unfortunately, the velocity signal from the motor is very noisy, so it would have to be averaged to smooth it. The filtering would tend to add a time delay to the inertial response. The inertia is particularly noticeable at the first few moments of motion, which is when the motor would have to be most responsive to the sudden change in movement. Consequently, it is very difficult to realistically simulate inertial effects and it requires a very large motor. Providing accurate inertia in the system with a flywheel eliminates these concerns and passively avoids the issues that would arise trying to do this electronically.

4. Methods

This section covers the implementation of the bicycle. This breaks down to the following tasks: selecting the bicycles, simulating kinetic energy, simulating wind resistance, connecting the inertial system to the bicycle, spinning the front wheel, measuring the steering angle, and organizing the electrical communications. The initial design concept (figure 1) highlights the kinetic energy and wind resistance simulation.

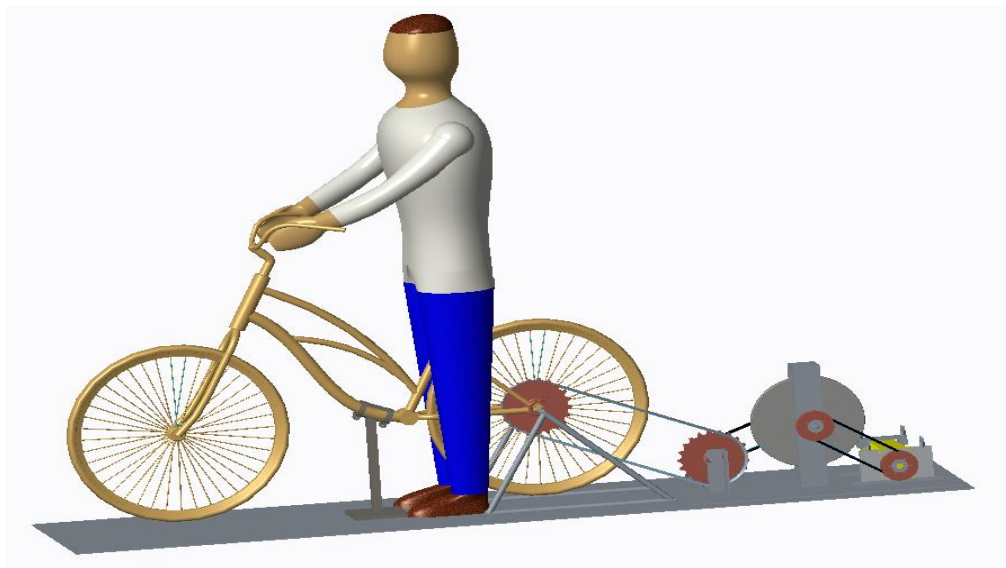


Figure 1: Initial design model. The inertial system behind the bike is exposed currently, but was enclosed for the final product.

4.1. Selecting the Bicycles

Bike selection consisted of two tasks: optimizing the quantity of rider heights captured while minimizing the number of bikes, and meeting predefined criterion established by the Hank Laboratory. The Hank Laboratory wanted the bikes to have a chain guard, be a step through bike, and have comfortable seats and cruiser handlebars. Knowing that the youngest simulator riders would be six years old, height distributions were used to determine the smallest rider size. The maximum height of 6 feet was predetermined during the bike's planning phase.



Figure 2: CDC Charts showing stature-for-age and weight-for-age percentiles from ages 2 to 20 years.

Children's bikes are sized by the diameter of the wheel, with typical sizes being 12, 16, 20, and 24 inches. 20-inch bicycles fit rider heights between 44 to 52 inches, while 16 inch bicycles fit rider heights between 38 and 47 inches. Comparing these heights to the CDC's stature-for age charts (figure 2), the 20-inch bike would fit 84% of 6-year-old girls, while a 16" bike fit the only the bottom 30% of kids. For this reason, the 20-inch bike was selected as the smallest. After this consideration, most of the remaining child riders were fit on the 24-inch bicycle. Adult riders, and larger children not captured by the 24-inch bike, were fit using a standard cruiser style bicycle which are designed to fit most adults.

4.2. Simulating Kinetic Energy

A flywheel mechanically connected to the bicycle was chosen to simulate the kinetic energy of the rider. By utilizing a mechanical connection, no lag would be present in the system allowing the pedal forces to be replicated instantaneously for the rider. To dimension the flywheel, the kinetic energy of the rider and the flywheel were set equal to each other. Let m be the mass of the cylindrical flywheel, r be the radius of the flywheel, ω be the rotational velocity of the flywheel, M be the mass of the rider, and v be the simulated bicycle velocity, then setting the inertial of the flywheel to be equal to the inertia of the rider:

$$\frac{1}{4} * m * r^2 * \omega^2 = \frac{1}{2} M * v^2$$

Since mechanical transfer system introduces a gear ratio factor G between the bike velocity and the flywheel rotation rate, such that $\omega = Gv/R$, where R is the radius of the rear wheel, then any rider mass can be simulated with an appropriate choice of flywheel mass, radius and gear ratio.

$$M = \frac{G^2 * m * r^2}{2 * R^2}$$

Thus, by introducing a variable gearing system and appropriate flywheel parameters, several masses in our target area may be simulated with a single flywheel. Since target masses have already been established, and rear wheel radii already selected, this leaves selecting an

appropriate gear ratio and flywheel for accurate simulation. The dimension combinations of the flywheel are theoretically limitless. Increasing and reducing the mass and radius allows an infinite quantity of flywheels to possess the same kinetic energy, as well as there being a flywheel to simulate any bodies' kinetic energy. For this reason, the gear ratios were selected before sizing the flywheel. An internally geared hub allows the simulator to change gears without pedaling, and offers a compact solution with more gears than offered in a typical cassette. An 11-speed internally geared hub was then selected with gear ratio ranges from 0.527 to 2.153. Using the gear ratios predefined by the hub, the ratio connecting the hub to the bike, and the flywheel, flywheel dimensions were selected.

Sizing the flywheel involved minimizing the weight and the radius of the flywheel to prevent the inertial system from being too heavy or clumsy to move. Using the upper and lower bounds of the masses and bike wheel radii, the flywheel (figure 3) was sized to 26 lbs. and 12.5" in diameter offering the best range of rider weights. This allows an upper bound of a 210-pound rider to be simulated on the 26-inch bicycle, and a lower bound of a 30-pound rider to be simulated on the 20-inch bike. The largest gap in simulated weights is from 165 pounds to 210 pounds, a 45-pound gap. This means the farthest difference of simulated weight versus rider weight is 22.5 pounds. The major downside of the flywheel is that simulated weights are limited to a discrete set of values. The set of values is defined by the gear ratios possible between the pedal and the flywheel. With the internally geared hub having 11 gear ratios, this offers 11 different simulated weights for each of the three bikes providing 33 unique combinations.



Figure 3: Flywheel with mounting brackets for the drive shaft.

4.3. Simulating Wind Resistance

To further improve the accuracy of simulation, a motor has been connected to the rear wheel through a chain and gearing hub. The motor is used to replicate drag caused by air. The drag equation is as follows:

$$F_D = \frac{1}{2} * \rho * v^2 * C_D * A$$

where F_D is the force of drag, ρ is the density of air, v is the velocity of the object, C_D is the drag coefficient, and A is the cross-sectional area. Values for the drag coefficient and the cross-

sectional area of rider on a commuter style bike are estimated to be 1.1 and 0.51 respectively. The velocity term can be derived from the motor which outputs its angular velocity to the motor controller. By passing this to a microprocessor the signal can be translated to simulated rider velocity. Then translating this to an equivalent torque, it is sent back to the motor to be outputted against the rotation of the flywheel, working against the rider's input force to simulate wind resistance. With the wind resistance and the kinetic energy simulated, all components of the target inertial system were designed. The resulting design was then modeled using CAD (figure 4).

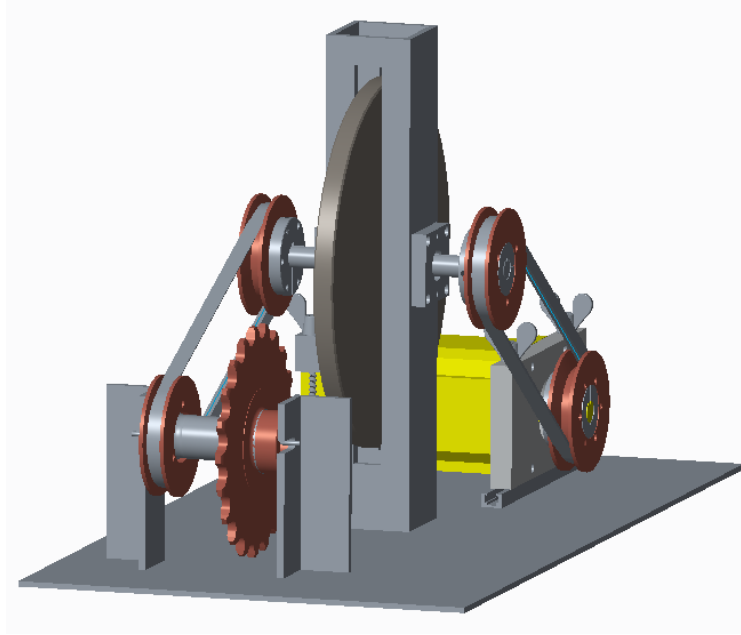


Figure 4: CAD model of the completed inertial system model. On the left is the internally geared hub. The center shows the flywheel. The right shows the motor (yellow).

4.4. Integration with Bikes

The flywheel is connected to the bike using a series of gears. A gear attached the flywheel's drive shaft is attached by chain to a sprocket on the internally geared hub, which is connected to the bicycle by chain. To connect the bicycle to the internally geared hub, a flip-flop hub

(figure 5), which is used in tandem bikes, was laced to the rear wheels of all the bicycles. The flip-flop hub offers a freewheel connection from the bike's pedals to the rear wheel, and a fixed connection on the non-drive side. The non-drive side is then connected by chain to the internally geared hub.



Figure 5: Flip-flop hub laced to a bike's rear wheel. The drive side (right) attaches to the pedals of the bike, where the non-drive side connects to the inertial system.

The internally geared hub (IGH) freewheels on the standard input side. The other side has a mount for disc brakes, with a circle pattern of screw holes to attach the brake. Using a custom adapter, a sprocket was attached to the IGH using the brakes mount. The freewheel side of the IGH was connected to the flip-flop hub so flywheels rotation would not spin the rear wheel. This results in the energy of the motor and the flywheel to be limited to only the inertial system and not potentially threatening the safety of the rider. The fixed side of the IGH is connected then by chain to the flywheel.

To connect the flywheel to the motor, identical pulleys were mounted to the drive shaft of the flywheel. These are connected by a timing belt to help prevent unintentional slipping. With the bike and the flywheel connected to the motor, the flywheel and the IGH needed to be supported so they may spin freely. Using two L brackets with milled slots, it was raised from the ground. The flywheel was supported using a large square tube with a milled slot running down parallel faces. Holes for the drive shaft were milled on the parallel two faces. The flywheel is slid into the milled slot, and then held up by the drive shaft which rests on bearings allowing smooth rotation. These supports are shown in figure 6.

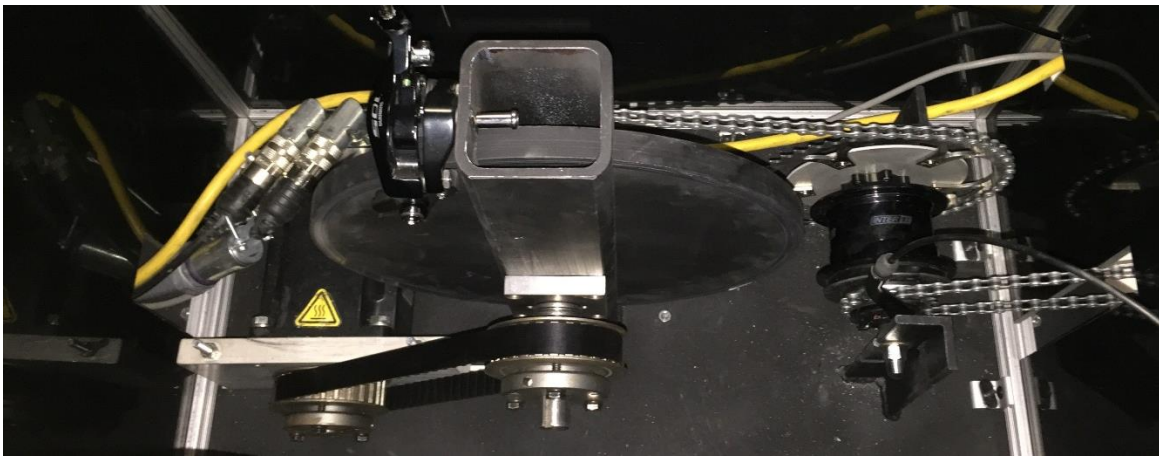


Figure 6: Manufactured inertial system for the bicycle. To the left is the motor which simulates wind resistance. The center shows the flywheel with a caliper break for speed control. The right shows the internally geared hub offering 11 gear ratios.

After considering how to attach the bicycle to the flywheel, the bicycle needed to be raised off the ground to allow the front and the rear wheels to spin. Commercial products were preferred for time and monetary savings. To lift the rear wheel from the ground, many commercial stands are available for purchase. A trainer styled stand was selected (figure 7) to lift the rear wheel for its price, sturdiness, and lack of training requirements. The stand grabs the

axle of the rear wheel to lift the back tire from the ground making it compatible with many styles of bicycles.



Figure 7: 26-inch bike with rear wheel stand attached.

Commercial products for lifting the front wheel off the ground did not offer the same safety that the rear wheel stand did, so a custom stand was fabricated (Figure 9). The stand extends from the floor and grabs the downtube of the bike. To ensure the stand wouldn't cause the downtube to buckle, the following stress calculations were performed to ensure the bike frame would not buckle when the frame was lifted from the down tube. They are as follows:

$$M_z = \frac{Pab^2}{L^2}$$

where M_z moment about the z axis, P point load on the tube, a and b are the distances from each end of the tube to P , and L is total length of the tube.

To calculate the moment of inertia about the z-axis:

$$I_{zz} = \pi \frac{d_o^4 - d_i^4}{64}$$

where d_o outer diameter of the tube, and d_i inner diameter of the tube. Using this and the moment caused by an axial force the stress, σ , placed on the tube is:

$$\sigma = \frac{M_z y}{I_{zz}}$$

Finally, the factor of safety can be calculated to evaluate the stand.

$$FoS = \frac{\text{Material Strength}}{\text{Stress } (\sigma)}$$

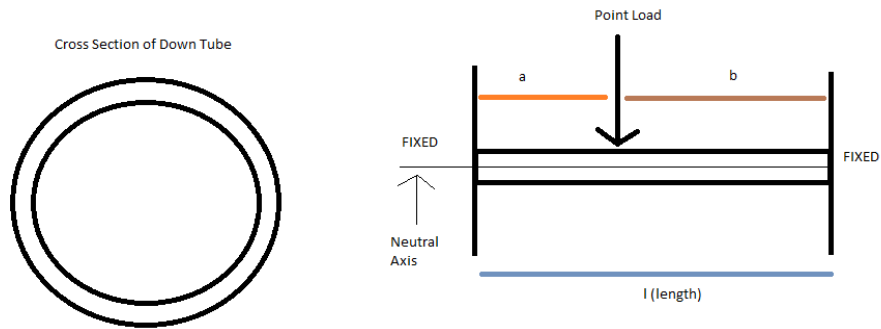


Figure 8: The cross section of the down tube as well as the model of the load on the downtube.

Factor of Safety	a (m)	b (m)
2	0.376016	0.490984
3	0.281034	0.585966
4	0.234203	0.632797

Table 2: Factors of Safety with their corresponding placement on the downtube.

A factor of safety of four is reasonably attainable for this stand, and considering the overestimations made during the calculations the actual factor is safety is higher. With the inertial system connected to the bicycle, and the bicycle raised off the ground the pedal forces can be appropriately simulated and the rider's velocity can be calculated.



Figure 9: Stand to lift the bicycles front wheel off the ground.

4.5. Spinning the Front Wheel

The front wheel will be spun using an electric hub motor. This was selected as it is electronically controllable and comes already attached to a wheel. This allowed avoiding a more time consuming and costly custom implementation. Electric hub motors are controlled using a twist or push throttle, sending a voltage signal to its motor controller. Depending on the voltage input, the controller then activates the motor to send at the desired speed. By reverse engineering the throttle, it was determined the signal sent varied was an analog, direct current voltage signal

varying between 0 and 5 volts. If the signal was 0 volts the motor would not spin, if it was 5 volts the motor would spin as fast as possible.

To simulate this signal, an Arduino Uno microcontroller was used. Though the Uno can only output 0 or 5 volts, it is capable of rapidly alternating between the two voltages in a technique called pulse width modulation. This allows replication of analog signals by digital means. Using a capacitor, the signal can be smoothed to appear as a DC signal. Then by changing the time between 5V pulses, the Arduino can simulate a continuous range of voltages using only the two discrete values. The circuit used is shown below.

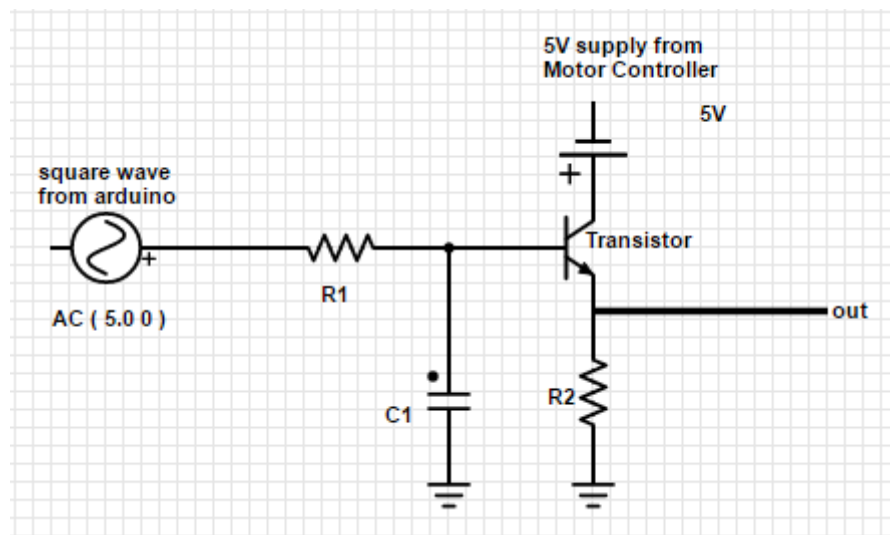


Figure 10: Circuit used to smooth the PWM signal from the Arduino.

Pulse width modulation (PWM) on the Arduino is a function that takes an input range of 0 to 255. Response from the motor was not observed until approximately a 1.92-volt signal, or an input of 98, was sent to the controller. The response speed continued to increase until 3.62 volts, or an input of 185 was reached, where no additional voltage output resulted in faster rotation. Using this, PWM values were plotted relative to the rotation speed of the wheel. The rotational

speed was measured using a tachometer, then to miles per hour using the diameter of the wheel to allow direct conversion from biker speed to the appropriate PWM value.

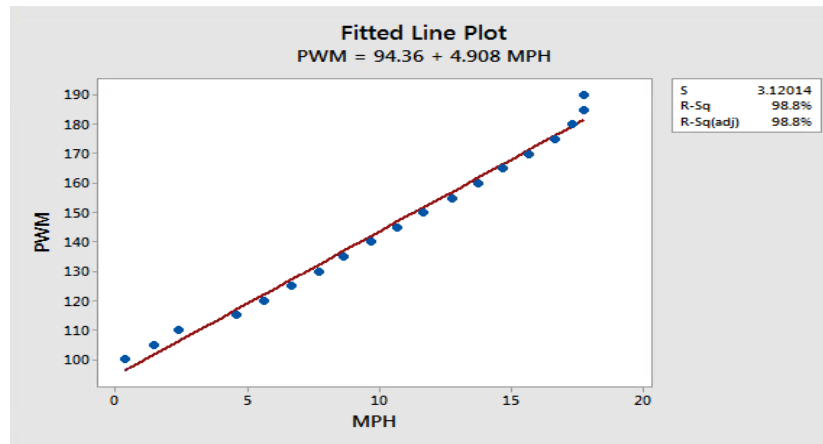


Figure 11: MATLAB figure showing best fit relation between MPH and PWM signal.

By using least squares regression, an equation relating PWM values to a certain MPH was established for each wheel size. The example above shows the regression fit, using MATLAB, to derive the equation for the 20-inch bicycle. Now with a given speed output we can closely simulate an accurate front wheel speed that'd appear to the rider as though it is spinning in a real-world situation. A hub-motor already laced to the 24-inch bike's wheel is shown (figure 12).



Figure 12: Electric hub-motor laced to the front wheel of a bike.

4.6. Measuring Steering Angle

To measure the rider's steering angle a device had to be mounted either the handle bars or the front wheel. The target rotation takes place in the central axis of the bikes head tube. Front forks, which extend down from the head tube and hold the front wheel, have a small bend before connecting to the wheel. This made it difficult to measure steering angle from the front wheel. The other end of the front fork extends through the top of the head tube, and is connected to the head tube by large nuts that screw to the top of the fork. The threads the nuts screw to are commonly keyed. This allowed for the design of a custom pulley which connected to the keyed downtube for rotation. By connecting the spinning pulley to a potentiometer or encoder, a voltage output could be read and translated into a steering angle.

Rotary encoders and optical encoders were considered, but the tested rotary encoders poor accuracy, and optical encoders flimsy design and difficulty to use. Consequentially, to maintain design strength yet still allow accurate measuring a potentiometer was selected. A custom mount to statically fix the potentiometer was made. The mount clamps around the bicycle's head tube and supports the potentiometer. By then attaching a pulley to the potentiometer and connecting it by belt to the custom pulley it would be spun by rotation of the handlebars. The two pulleys have a resulting gear ratio which allows conversion from the potentiometer's voltage output to a steering angle. This voltage is read by an Arduino Uno and outputted to the bicycle simulator.

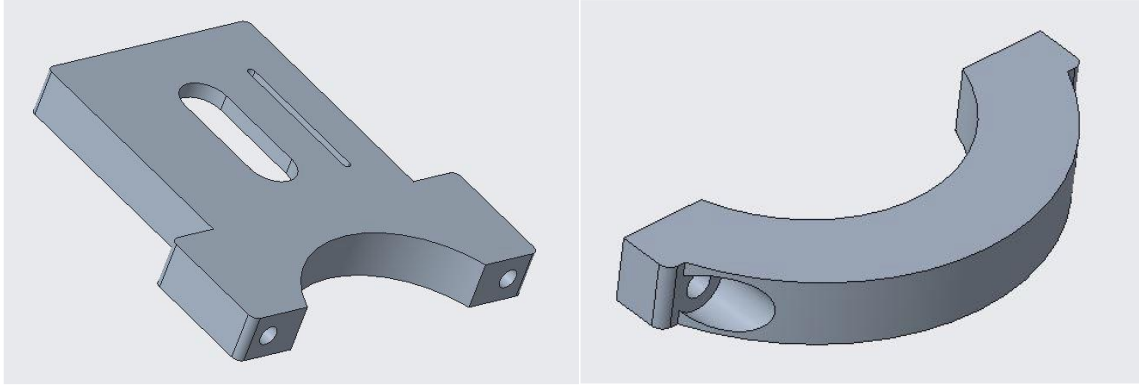


Figure 13: Mount designed to connect potentiometer to a bicycle's head tube.

Knowing the effective electrical angle of the potentiometer, and its maximum voltage output, the angle change per volt can be calculated. By multiplying this number by the gear ratio and the measured voltage deviation from when the bike is moving straight forward, the handle bar rotation can be calculated. The final potentiometer mount (figure 14) was made with a cover to hide the system from the simulated subject.



Figure 14: Potentiometer mount with (left) and without (right) the cover.

4.7. Electrical Communication

An Arduino Uno microcontroller was used to coordinate the electrical communication between the rear motor controller, the front motor controller, the potentiometer, and the computer science computer. The diagram below shows the data flow between each of the devices.

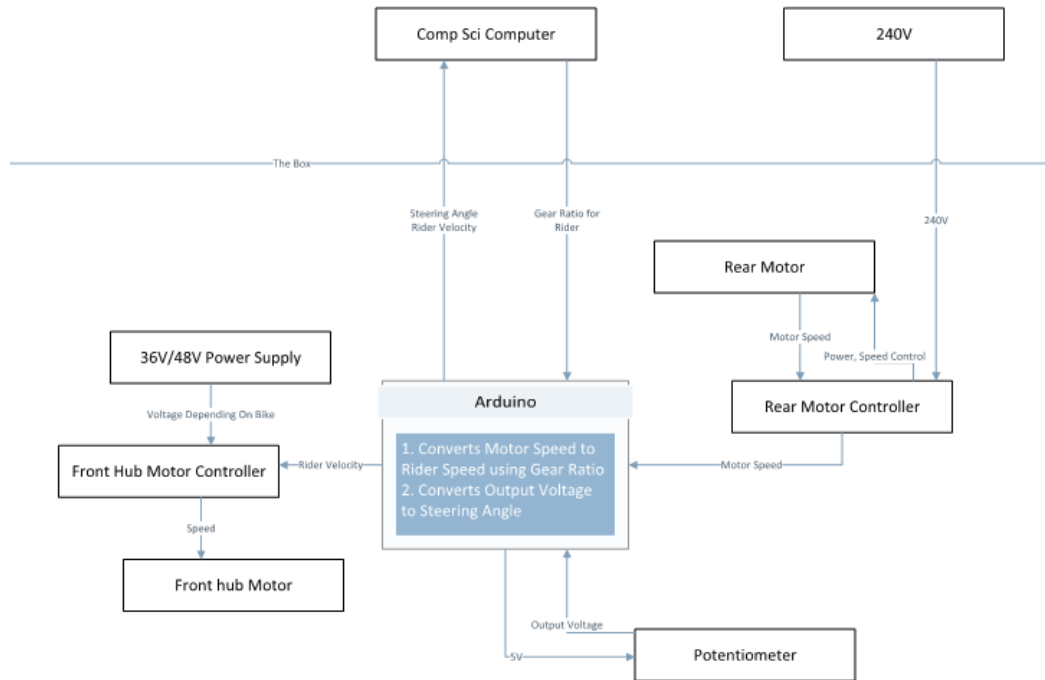


Figure 15: Wiring diagram and data flows for the bicycle.

The Uno reads from the potentiometer, the rear motor controller, and the Hank simulator. It then converts the voltage output from the potentiometer to the steering angle, and the motors angular velocity to the rider's speed. After conversions are made it outputs the steering angle and rider velocity to the simulator for display. It also outputs the voltage corresponding to the rider's speed to the front hub motor controller to spin the front wheel. The rear motor controller is powered by a 240-volt wall outlet, the front motor is powered with a 36 or 48-volt power supply

depending on the hub motor's size, and the Arduino is powered by the data transmission line connecting it to the simulator.

5. Results

The resultant theoretical electro-mechanical system is compatible with the three selected bike frames and can handle rider speeds of up to 25 mph. It can simulate inertia for riders ranging from 30-275 pounds, based on the 11 gears that are used through the internally geared hub and the gear ratio from the rear wheel to the flywheel. The largest possible difference between actual and simulated weight is 22.5 pounds. The bicycle's handle bars rotate freely in a range of 175 degrees and the steering angle is measurable and easily collected. The front wheel spins at speeds relative to the rider's simulated speed. The completed assembly, fitted with a 24-inch bicycle is pictured below.



Figure 16: The completed stationary bike, with the inertial system enclosed behind the bicycle.

References

- Babu, S., Grechkin, T., Chihak, B., Ziemer, C., Kearney, J., Cremer, J., & Plumert, J. (2009). A Virtual Peer for Investigating Social Influences on Children's Bicycling. *IEEE Virtual Reality*, 91-98.
- Centers for Disease Control and Prevention (2016). Web-based Injury Statistics Query and Reporting System (WISQARS). Atlanta, GA: Centers for Disease Control and Prevention, National Center for Injury Prevention and Control.
- Grechkin, T.Y., Chihak, B.J., Cremer, J.F., Kearney, J.K., & Plumert, J.M. (2013). Perceiving and acting on complex affordances: How children and adults bicycle across two lanes of opposing traffic. *Journal of Experimental Psychology: Human Perception and Performance*, 39(1), 23-36.
- He, Q., Fan, X., Ma, D. (2005). Full Bicycle Dynamic Model for Interactive Bicycle Simulator. *Journal of Computer and Information Science in Engineering*, 5(4), 373-380.
- Huang, S.F., Tsai, P.Y., Sung, W. H., Lin, C. Y., & Chuang T.Y. (2008). The Comparisons of Heart Rate Variability and Perceived Exertion During Simulated Cycling with Various Viewing Devices. *Presence*, 17(6), 575-583.
- Kwon, DS., Yang, GH., Lee, CW., Shin, JC., Park, Y., Jung, B., Lee, D.Y., Lee, K., Han, SH., Yoo, BH., Wohn, KY., & Ahn, JH. (2001). KAIST interactive bicycle simulator. *Robotics and Automation. Proceedings 2001 ICRA. IEEE International Conference*, 3, 2313-2318.
- Kwon, DS., Yang, GH., Park, Y., Kim, S., Lee, CW., Shin, JC., Han, S., Lee, J., Wohn, K., Kim, S., Lee, D.Y., Lee, K., Yang, JH., Choi, YM. (2002). KAIST interactive bicycle racing

- simulator: the 2nd version with advanced features. *Intelligent Robots and Systems*, 2002. *IEEE/RSJ International Conference*, 3, 2961-2966.
- Leblanc, MA., & Sicard, P. (2010). "EMR and inversion-based control of a virtual reality bicycle trainer," *2010 IEEE Vehicle Power and Propulsion Conference*, 1-7.
- Mestre, D., Dagonneau, V., & Mercier, CS. (2011). Does Virtual Reality Enhance Exercise Performance, Enjoyment, and Dissociation? An Exploratory Study on a Stationary Bike Apparatus/ *Presence*, 20(1), 1-14.
- Miyanoue, K., Suzuki, M., Yai, T. (2015). Riding Performance Evaluation Of Cycling Simulator “Morics” Considering Rider’s Controllability. 1-10.
- National Center for Statistics and Analysis (2016). Bicyclists and other cyclists: 2014 data. (Traffic Safety Facts. Report No. DOT HS 812 282). Washington, DC: National Highway Traffic Safety Administration.
- Plumert, J. M., Kearney, J. K. and Cremer, J. F. (2004). Children's Perception of Gap Affordances: Bicycling Across Traffic-Filled Intersections in an Immersive Virtual Environment. *Child Development*, 75, 1243–1253.
- Plumert, J., Kearney, J., & Cremer, J.F. (2007). Children's Road Crossing A Window Into Perceptual–Motor Development. *Current Directions in Psychological Science*, 16.5, 255-258.
- Sari, R.F., Gianty, A., Parameswari, C. & Purnamasari, P. D. (2009). 3D object implementation on bicycling at ui virtual reality application based on 3D-Gamestudio. *2009 International Multiconference on Computer Science and Information Technology*, 509-515.

- Tang YM., Tsoi M.HC., Fong D.TP., Lui P.PY., Hui KC., Chan KM. (2007). The Development of a Virtual Cycling Simulator. *Technologies for E-Learning and Digital Entertainment*, 4469, 162-170.
- Wilson, G., & Papadopoulos, J. (2004). *Bicycling science*. Cambridge, Massachussets: MIT press.